A MEMS Actuator System for an Integrated 3-D Optical Coherent Tomography Scanner

Jovic, Aleksandar; Pandraud, Gregory; Sanchez Losilla, Nuria; Sancho, Juan; Zinoviev, Kirill; Rubio, Jose L.; Margallo Balbas, E; Sarro, Lina

DOI
10.1109/JMEMS.2018.2802321

Publication date
2018

Document Version
Final published version

Published in
Journal of Microelectromechanical Systems

A MEMS Actuator System for an Integrated 3-D Optical Coherent Tomography Scanner

Aleksandar Jovic, Grégory Pandraud, Nuria Sanchez Losilla, Juan Sancho, Kirill Zinoviev, Jose Luis Rubio, Eduaro Margallo-Ballbas, and Pasqualina M. Sarro, *Fellow, IEEE*

***Abstract*— In this paper, we present an electrothermal biaxial MEMS actuator system, which provides *x*- and *y*-direction scanning for a fully integrated 3-D optical coherence tomography (OCT) scanner. An angular scanning range of 8° (corresponding to a 7-mm linear scanning range in both directions) is achieved, with an average power consumption of 150 mW. The resonant frequency is 668 and 297 Hz for x- and y-directions, respectively. With a footprint of only 2.5 × 2.5 mm^2, this system is part of a device which also integrates an optical waveguide and a collimated lens on the same chip, thus making the fully integrated, self-aligned, and miniaturized 3-D OCT scanners feasible. [2017-0268]**

***Index Terms*— MEMS actuators, integrated OCT, Al – SiO_2 bimorph beam.**

I. Introduction

IN THE past decades the risk of skin cancer has significantly increased [1]. Successful treatment is highly dependent on melanoma detection in its early stage [2]. This requires physical skin removal by a medical specialist, a painful, invasive procedure, and a long waiting time for the result to be available. Alternative diagnostic methods are therefore needed. Among these, optical coherence tomography (OCT) is a non-invasive medical imaging technique, which provides live morphology of a patient tissue. In dermatology, OCT uses near infrared light for 3D *in vivo* tissue imaging up to a depth of 3 mm [3].

The OCT image is generated by measuring the optical path difference between a reference and a scattered beam in an interferometer setup. For 3D OCT imaging, optical scanning of the surface in both *x* and *y* direction, which translates into 2D motion of the light beam, is needed. Commercially available systems have large footprint (∼1 m^3) with an average cost of ∼100k$. Hence, a miniaturization of these systems to reach affordable, handheld probes is needed to guarantee a widespread use of these diagnostic tools to general practitioners and clinics.

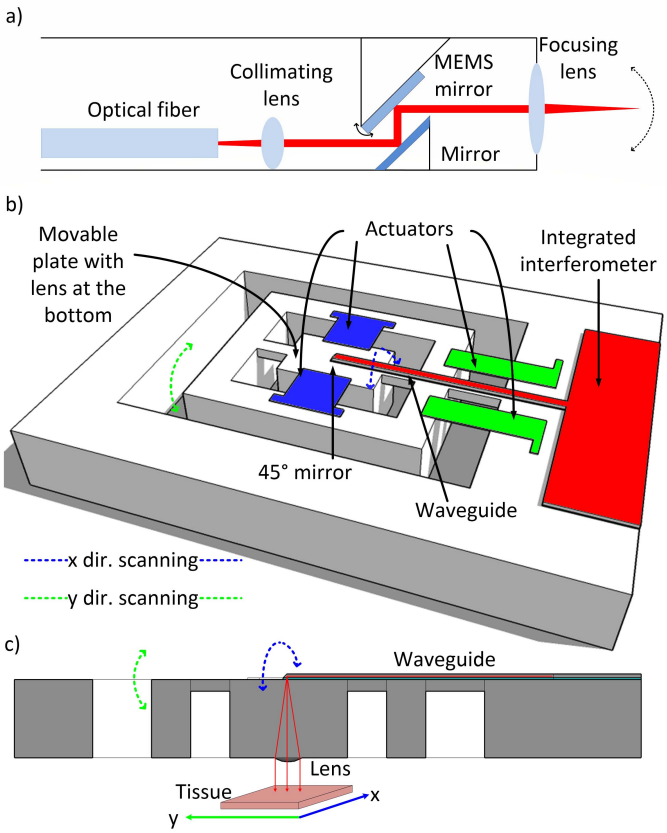

Fig. 1. Schematics drawings of (a) state of the art MEMS based OCT probe; (b) the self-aligned 3D integrated OCT scanner; (c) light propagation through the integrated OCT system.

A first step towards miniaturization of OCT scanners came along with the use of MEMS micro mirrors, which resulted in the first portable handheld imaging probes [4]. This miniaturized OCT system consists of several separate sub-systems for image generation (light source, photodetector and image processor), photonic circuitry (beam splitters, fibers etc.) and scanning (MEMS mirror and collimated lens). Figure 1a depicts a schematic drawing of a state of the art OCT scanner, where light is brought in using an optical fiber aligned with a MEMS mirror, a collimating and a focusing lens [4], [5].

Manuscript received October 27, 2017; revised December 30, 2017; accepted January 14, 2018. Date of publication February 22, 2018; date of current version April 2, 2018. This work was supported by the BiopsyPen Project, 7th Framework Programme of European Commission, under Grant 611132. Subject Editor O. Solgaard. *(Corresponding author: Aleksandar Jovic.)*

A. Jovic and P. M. Sarro are with the ECTM Group, Microelectronics Department, Faculty of Electrical Engineering, Mathematics and Computer Science, Delft University of Technology, 2628 CT Delft, The Netherlands (e-mail: a.jovic@tudelft.nl).

G. Pandraud is with the EKL Laboratory, Delft University of Technology, 2628 CT Delft, The Netherlands.

N. S. Losilla, J. Sancho, J. L. Rubio, and E. Margallo-Balbas are with Medlumics S.L., 28760 Madrid, Spain.

K. Zinoviev was with Medlumics S.L., 28760 Madrid, Spain. He is now with imec, 3001 Heverlee, Belgium.

Color versions of one or more of the figures in this paper are available online at http://ieeexplore.ieee.org.

Digital Object Identifier 10.1109/JMEMS.2018.2802321

Image quality and optical losses strongly depend on the accurate alignment of the components within the OCT probe package, which requires expensive and time-consuming procedures [6]. Hence, much research in this field has been focusing on the main limitations of these OCT systems, namely simplifying the assembly [7], improving the signal acquisition [8] and most importantly increasing the scanning range of the MEMS micro mirrors [4], [5], [9]. The alignment problem, which significantly contributes to the high overall system price, has barely been addressed so far.

In this paper we present a self-aligned integrated concept for surface scanning (Fig. 1b) [10]. The integrated system contains four sub-modules: a waveguide system, which replaces an optical fiber circuit for OCT interferometry; a 45° mirror facet, which scatters the light; a collimating lens, to collimate the light beam at the output of the system; and a MEMS actuator system which provides motion to the light on the scanning surface. The light propagation through the waveguide, the mirror and the lens are illustrated in Fig. 1c. The central wavelength for OCT imaging in dermatology is 1300 nm. Therefore, Si is suitable for the photonic circuit, the lens fabrication as well as for the MEMS actuator system.

Fabrication of all components on a single substrate makes the presented concept a fully integrated OCT scanning device. To achieve this, all four components must be compatible, both from the design and from the fabrication point of view. A time domain OCT system working at a speed of 10 Hz must have at least 10 times higher resonant frequency, to disregard for hand tremor influence on the image quality. A handheld device needs components with the smallest footprint possible and low voltage operation. Still, the most important parameter is the optical scanning range, which corresponds to large displacement for the actuator system.

The first criteria for choosing the right actuator type is the nature of the motion, which for the proposed systems, is an out-of-plane and tilting motion. Comb drive electrostatic actuators are widely used as in-plane actuators, and with a specific design it is possible to generate rotational motion [11]. However, the footprint of comb drives is large, and the drive voltage is high [11], [12]. Magnetic MEMS actuators require an external magnetic field and dense metal lines for increasing the electromagnetic force on the plate [9], [12], [13]. Finally, electrothermal bimorph actuators are by their nature out-of-plane actuators [12]. They provide a large displacement range, require low operating voltage and provide a large output force [5], [12], [14]. The most commonly used material layers combination is Al and SiO_2, due to the large difference in coefficient of thermal expansion [15]–[17]. Further, their integration with optical circuit has already been demonstrated in [18]. Electrothermal Al-SiO_2 bimorph cantilevers satisfy all mentioned requirements, making them the most suitable candidate for this application.

To fabricate the fully integrated OCT scanning systems, all components must be first fabricated and tested individually. Low loss (0.13 dB/cm) waveguides defined in the SOI device layer are reported in [19], while the mirror fabrication is defined in [20] and Si lenses with roughness of only 25 nm are presented in [21]. In this paper, the focus is on the system design considerations and thermal characterization of the MEMS actuator system introduced in [22].

To investigate the feasibility of the system depicted in Fig. 1b, separate designs (sect. II) for linear scanning in x and in y direction are considered. Numerical analysis and optimized design parameters for the two actuator systems are presented (sect. II). The fabrication flow is briefly described (sect. III), and the device static response, thermal characterization and frequency response are reported and discussed (sect. IV).

II. The MEMS Actuator System Design

Commercially available 3D OCT scanners can cover a surface area of up to 1 cm^2. For our system, this translates into a 12° of tilting/deflecting motion for both scanning directions. For this purpose, the actuator system must be designed and simulated to determine its thermal and mechanical properties.

First, the x direction scanning system is defined and then, based on this system, a compatible y direction scanning system is determined. Horizontal scanning, i.e. in the x direction, is provided by rotating the lens around torsional hinges, while y direction (i.e. vertical) scanning is generated by deflecting the supportive hinge of the lens. The waveguide runs along both hinges. The combination of these two actuator modules into one device allows 3D OCT imaging (Fig. 1b).

The residual stress values used for numerical simulation are based on experimental findings for bimorph beams made of 2 μm-thick Al film sputtered at 350 °C and 2 μm-thick PECVD SiO_2 film deposited at 400 °C, which are the same layers used for the actuator beams. Stress values of 100 MPa for Al and 40 MPa for SiO_2 tensile were measured. All simulations are done using COMSOL Multiphysics 4.4.

A. Actuator Design for x Direction Scanning

To create a torsional motion around the waveguide with Al-SiO_2 electrothermal bimorph actuators, these beams must be placed on each side on the microplate which contains the lens and the 45° mirror. Actuators on both sides are prestressed and have an initial deflection. Both sides are pushing the microplate with force F_0 at its edge and since both sides are at the same distance from the torsional axis, the plate has no angular displacement (Fig. 2a). Once one side is operated using Joule heating, the actuators will move upwards. Hence, the applied force F_a is lower than F_0, which results in a rotation around the torsional axis. The heated bimorph now acts like a spring with a constant k_b (Fig. 2b). In the final state, i.e. for the maximum torsional displacement, the force F_a equals to zero. The whole rotation is now generated with force F_0 from the non-actuated beam (Fig. 2c).

By the third Newton's law, a reaction force F_r is applied to the actuator in the opposite direction than F_0. In the final state, the not heated actuator deflection, d_{max}, is determined by residual stress in the beam after fabrication (including proper burn-in process) and the reaction force Fr from the plate. The maximum angle is defined by the deflection d_{max} of the beam and the distance from the actuator tip to the torsional axis (w_p/2). This is illustrated in Fig. 2c.

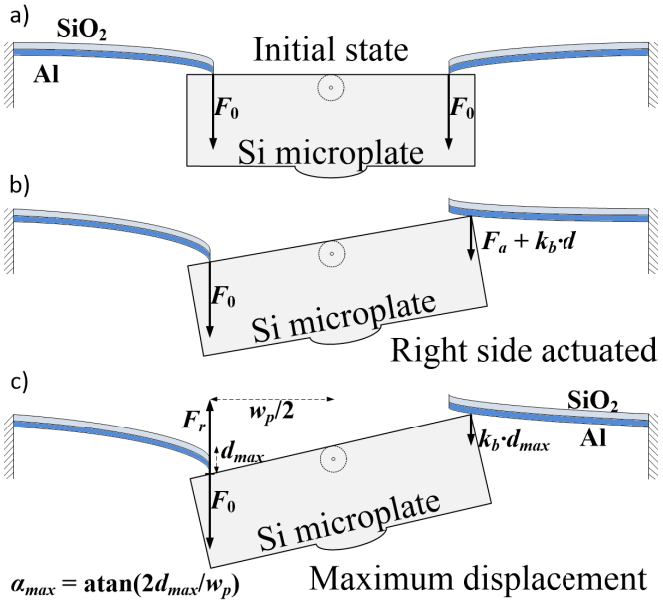

Fig. 2. Working principle for x direction scanning OCT system using Al-SiO_2 electrothermal bimorph cantilevers: (a) Initial state where both group of actuators are applying the same force. (b) Right side is actuated, and cantilevers are bending up resulting in lower force applied to the plate. (c) Maximum torsional angle in the final state of the actuation.

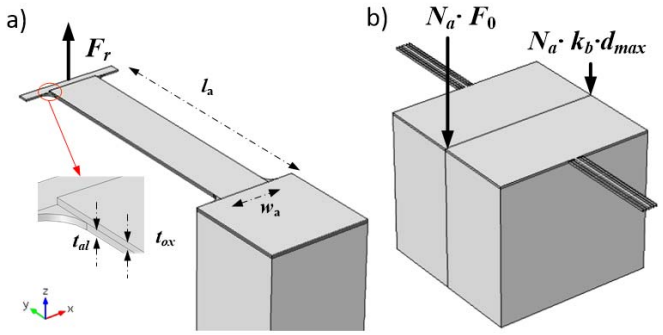

Fig. 3. (a) Geometric parameters used for the simulation model of an electrothermal actuator beam. (b) 3D simulation model for a microplate supported by torsional hinges.

In Fig. 3a the simulation model of an electrothermal bimorph beam actuator is depicted. The length of the beam, l_a, is varied from 300 μm to 800 μm, the width, w_a, from 50 μm to 150 μm, while layer thickness, t_{al}, of Al and t_{ox} of SiO_2 from 1 μm to 3 μm. In the simulation model a point force F_r is applied at the end of the beam to investigate the beam flexibility in the vertical direction, i.e. its spring coefficient k_b.

Numerical simulations of the maximum actuator tip displacement, d_{max}, caused by the residual stress and applied force F_r for different values of l_a, w_a, and the total actuator thickness $(t_{al} + t_{ox})$ give the actuator spring coefficient value k_b (Fig. 3a). The Young's moduli of Al and SiO_2 are close, respectively 70 GPa for Al [23] and 75 GPa for SiO_2 [24]. Therefore, similar elastic properties are expected between beams of 1 μm of Al and 3 μm of SiO_2 or 3 μm of Al and 1 μm of SiO_2. We are interested only in the linear regime of the actuator deformation when a force F_r is applied, i.e. when

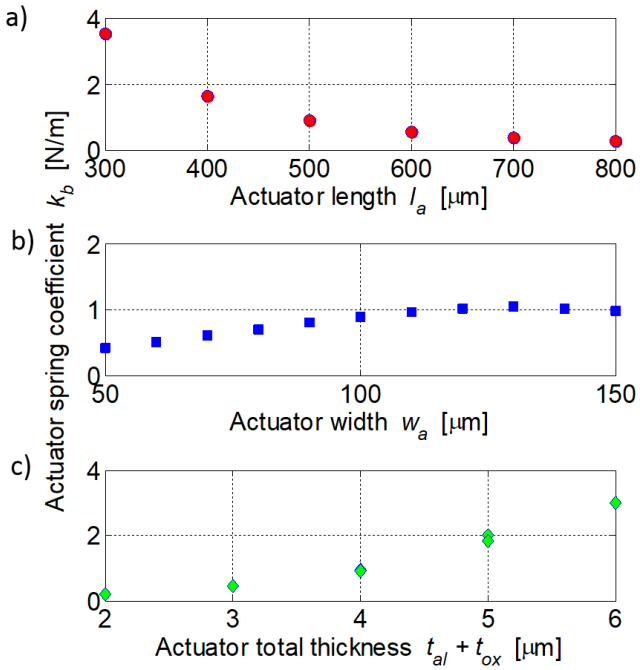

Fig. 4. Calculated spring coefficient k_b for (a) varying actuator length when w_a is 100 μm, t_{al} is 2 μm, t_{ox} is 2 μm; (b) varying actuator width when l_a is 500 μm, t_{al} is 2 μm, t_{ox} is 2 μm; (c) varying layer thicknesses when l_a is 500 μm and w_a is 100 μm.

Hook's law is valid. For each length, width or total bimorph layer thickness, the spring coefficient of the beam is calculated and is given in Fig. 4.

If the actuator spring coefficient is higher, the delivered force F_0 is also higher (Fig. 2c). However, the resistive force $k_b \cdot d_{max}$ (Fig. 2c) is also higher. For the range of thicknesses considered, a total thickness of 4 μm is chosen as a trade-off between flexibility and generated force. Based on the analysis carried out in [5], the optimal ratio of layer thickness should be equal to the square root of layer biaxial Young's moduli. We selected a total thickness of 4 μm, in which the Al layer should be 1.965 μm, while the SiO_2 should be 2.035 μm. This difference is almost negligible and to ease fabrication, the thickness for both layers is fixed at 2 μm. Similarly, the actuator width w_a is set at 90 μm and the length l_a at 500 μm.

The next step, the dimensioning of the MEMS actuator system concerns the plate width w_p and the number of actuators N_a on each side. The inclusion of both actuators with plate and hinges makes the 3D FEM model complex for numerical calculation. The maximum angular displacement is defined in the steady state of the system, as illustrated in Fig. 2c. Therefore, the numerical computation can be divided in two parts: the actuator displacement calculation and the plate rotation calculation.

For a chosen geometry of the actuator, the calculation of the vertical displacement versus applied force is done using the model given in Fig. 3a. The simulation showed that the required power per actuator to achieve an average temperature of 260 °C is estimated to be 70 mW (Fig. 5).

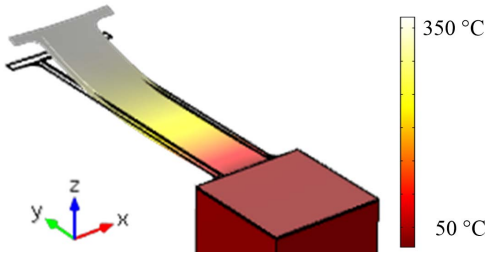

Fig. 5. Temperature distribution in an Al-SiO_2 bimorph cantilever for 70 mW applied power.

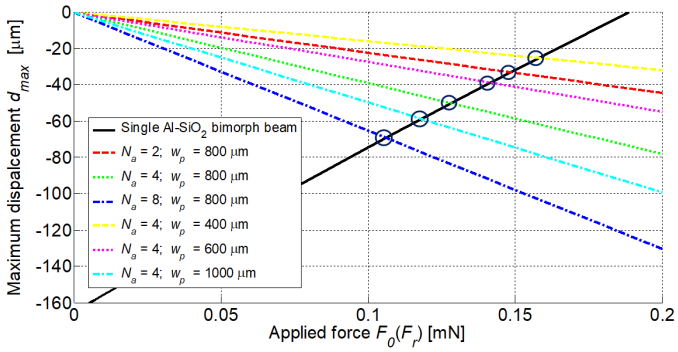

Fig. 6. Dashed lines represent the maximum displacement of the microplate for several combinations of N_a and w_p as function of the applied force F_0. The intersections with the maximum deflection of the actuator tip (circles) versus F_r (solid line) give the possible combinations for maximum displacement of the system.

At this temperature, the actuator stops pushing the plate further (see Fig. 2c).

A geometrical model of the plate with force distribution is given in Fig. 3b where N_a is number of actuators on each side and k_b is the calculated elastic spring constant of the actuator. Thermal changes of Young's modulus are neglected here. Although this assumption is not valid for the temperature range used as indicated in [25], the discrepancy is in a first order analysis acceptable.

Figure 6 reports the simulation results of d_{max} as a function of F_0 or F_r. The solid line represents d_{max} versus F_r for the actuator tip, while the dashed lines represent the dependency of d_{max} versus F_0 for the edge of the plate for several combinations of N_a and w_p. The intersection points indicate possible combinations for the maximum displacement of the system. The angular displacement is calculated based on these values for F_0 and N_a for different combinations of w_p.

Figure 7 shows the angular displacement α_{max} versus the number of applied actuators N_a when w_p is set to 800 μm (Fig. 7a), and versus plate width w_p with $N_a = 4$ actuators on each side (Fig. 7b)). As expected, more actuators can generate a larger angular displacement. However, more actuators would linearly increase the power consumption, while it would not linearly increase the generated angular displacement. An acceptable tradeoff between increasing α_{max} and reducing the power consumption is to have 4 actuators on each side of the plate. For $N_a = 4$, a maximum angular displacement of 6.16 ° is achieved for a plate width of 800 μm.

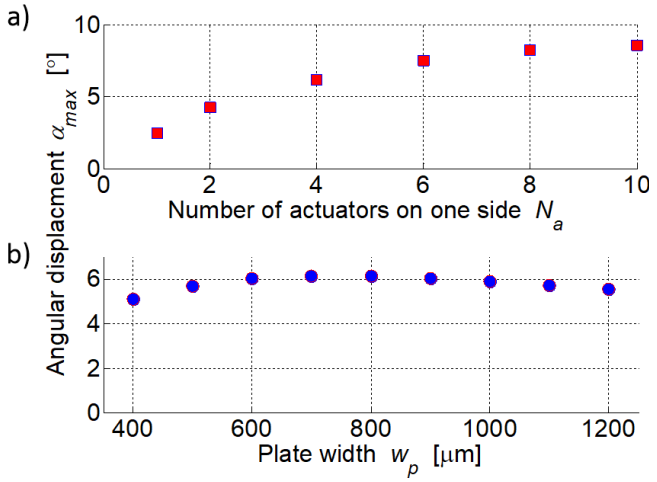

Fig. 7. Angular displacement versus (a) number of actuators for $w_p = 800$ μm and (b) plate width with $N_a = 4$ actuators per side.

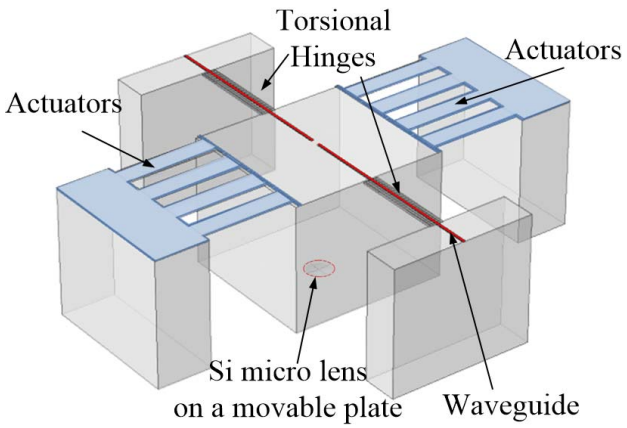

Fig. 8. Final design of the MEMS actuator system for x direction scanning together with the optical components for OCT imaging. Reproduced with permission form [22].

Each group of 4 actuators must be placed 400 μm away from the central axis on each side.

In Fig. 8 the final 3D model of the MEMS actuator system with 4 actuators on each side is depicted. The microplate has a lens at the bottom and is supported by two torsional hinges. A waveguide with a 45° ending facet runs along the hinges. Design parameters and expected working parameters for the MEMS actuator system for x directional scanning are summarized in Table 1.

B. Actuator Design for y Direction Scanning

For the y direction scanning system (Fig. 1b), the same Al-SiO_2 electrothermal bimorph beam actuators can be used in the configuration given in Fig. 9. Also in this case, the system has a deflecting hinge carrying a waveguide. Initially, actuators and hinge are deflected due to residual stress of the actuators, thus giving an initial angular displacement of the plate (Fig. 9a). Using Joule heating, hinge and actuators will deflect in the opposite direction, rotating the plate at the same time. This is illustrated in Fig. 9b.

TABLE I
PARAMETERS OF THE MEMS ACTUATOR SYSTEM FOR X DIRECTION SCANNING

Symbol	Quantity	
l_a	actuator length	500 µm
w_{al}	Al layer width	110 µm
t_{al}	Al layer thickness	2 µm
w_{ox}	SiO_2 layer width	90 µm
t_{ox}	SiO_2 layer thiskness	2 µm
N_a	number of actuators per side	4
g_a	gap between actuators	90 µm
l_h	hinge length	500 µm
t_h	hinge thickness	60 µm
w_{hc}	central hinge width	15 µm
w_{hs}	side hinge width	5 µm
g_h	gap between hinges	10 µm
w_p	microplate width	840 µm
l_p	microplate length	800 µm
α_{max}	maximum angular displacement	±6.16°
P_{max}	maximum power consumption	280 mW
T	average working temperature	260 °C
f_r	resonant frequency	534 Hz

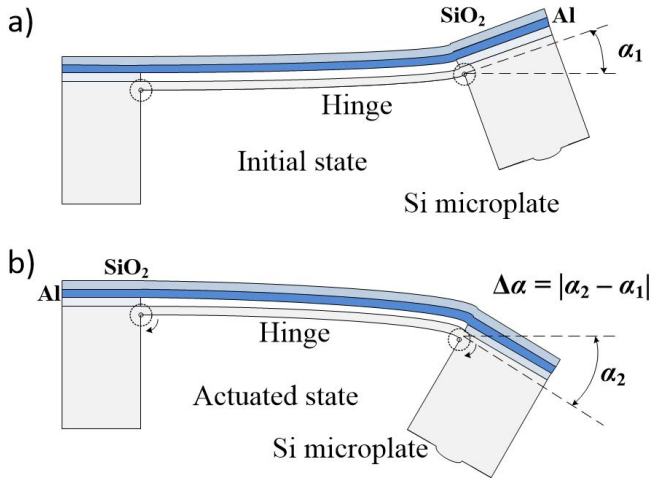

Fig. 9. The y direction MEMS scanning system: (a) Initial; (b) Actuated state.

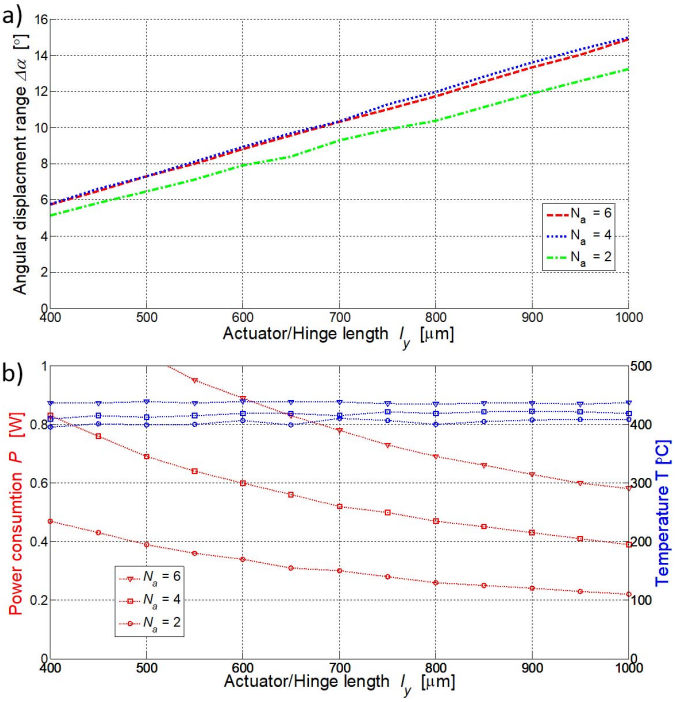

Fig. 10. (a) Angular displacement range (b) Power consumption and working temperature versus actuator/hinge length for $N_a = 2$, 4 and 6.

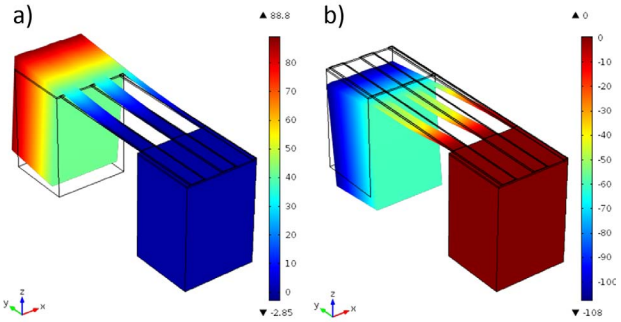

Fig. 11. Simulation results for $N_a = 4$ and $l_y = 800$ μm: (a) initial microplate position due to pre-stress and (b) final microplate position at 420 °C. (Only one half of the system is simulated to save computational time).

This system needs to be compatible with the previously designed x direction scanner. Therefore, the type and thickness of the bimorph layers should be the same as for the x direction scanner. The only two parameters here optimized for the desired motion range of 12° are the number of actuators and the actuator/hinge length.

To find the desired number of actuators N_a, a system with 2, 4 and 6 actuators is analyzed. To choose the best actuator/hinge length l_y, this parameter is varied between 400 μm and 1000 μm. The maximum displacement angle range versus actuator/hinge length is reported in Fig. 10a. The motion range of 12° is achievable using different combinations of N_a and l_y. In Fig. 10b temperatures and power consumption to achieve the final position of the microplate in the actuated state are presented.

The system with 2 actuators and hinge length of 900 μm uses 250 mW of power to provide the desired motion range. However, this configuration could result in low resonant frequency. The system with 4 actuators needs a hinge of 800 μm length for the same motion range but it uses 470 mW of power. Increasing the number of actuators to 6 could increase the power consumption to 690mW and the eigenfrequency of the system, while still needing the same hinge length for a 12° angular range. Therefore, the configuration with 4 actuators and a length l_y of 800 μm is chosen as a tradeoff between mechanical performance and power consumption. Simulation results for this configuration are shown in Fig. 11.

The final 3D design model for the MEMS actuator system for y direction scanning is presented in Fig. 12. The system has 4 actuators, 2 on each side of the deflecting hinge. Also in this case a 3 × 3 μm^2 Si waveguide with a 400 nm-thick SiO_2 layer underneath is placed on the top of the hinge and ends with a 45° facet above the Si microlens. Design parameters and expected operational values are summarized in Table 2.

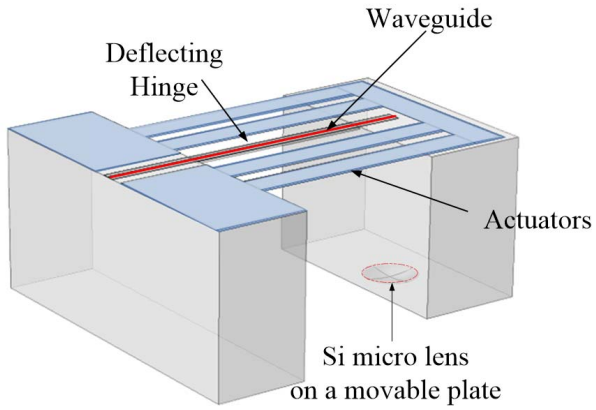

Fig. 12. Final design of the MEMS actuator system for y direction scanning with optical components for OCT imaging. Reproduced with permission form [22].

TABLE II
PARAMETERS OF THE MEMS ACTUATOR SYSTEM FOR Y DIRECTION SCANNING

Symbol	Quantity	Value
l_y	actuator/hinge length	800 µm
w_{al}	Al layer width	110 µm
t_{al}	Al layer thickness	2 µm
w_{ox}	SiO_2 layer width	90 µm
t_{ox}	SiO_2 layer thickness	2 µm
N_a	number of actuators per side	4
g_a	gap between actuators	115 µm
t_h	hinge thickness	10 µm
w_{hc}	hinge width	60 µm
w_p	microplate width	800 µm
l_p	microplate length	450 µm
α_{max}	maximum angular displacement	±6°
P_{max}	maximum power consumption	470 mW
T	average working temperature	420 °C
f_r	resonant frequency	463 Hz

As mentioned, this system is designed to achieve a motion range of 12° along y. The chosen geometry is a tradeoff between power consumption and eigen frequency.

III. DEVICE FABRICATION

The waveguide system for the Si-based photonic interferometer for the OCT scanner utilizes the device layer of a silicon-on-insulator (SOI) wafer. Consequently, for a fully integrated chip, the other components and the hinges need to be built in the bulk silicon. The fabrication process for the MEMS actuator systems must be compatible with the already developed technology for photonic integrated circuit (PIC) [19], mirror [20] and Si micro lens [21]. The process flow can be separated into two modules: the bimorph definition and the hinge definition.

The fabrication of the MEMS actuator system starts with the deposition of a sacrificial layer (3 μm-thick SiO_2) for device final release, namely by silane-based plasma enhanced chemical vapor deposition (PECVD). This layer also serves as insulator for the heater, which is made of a 300 nm-thick

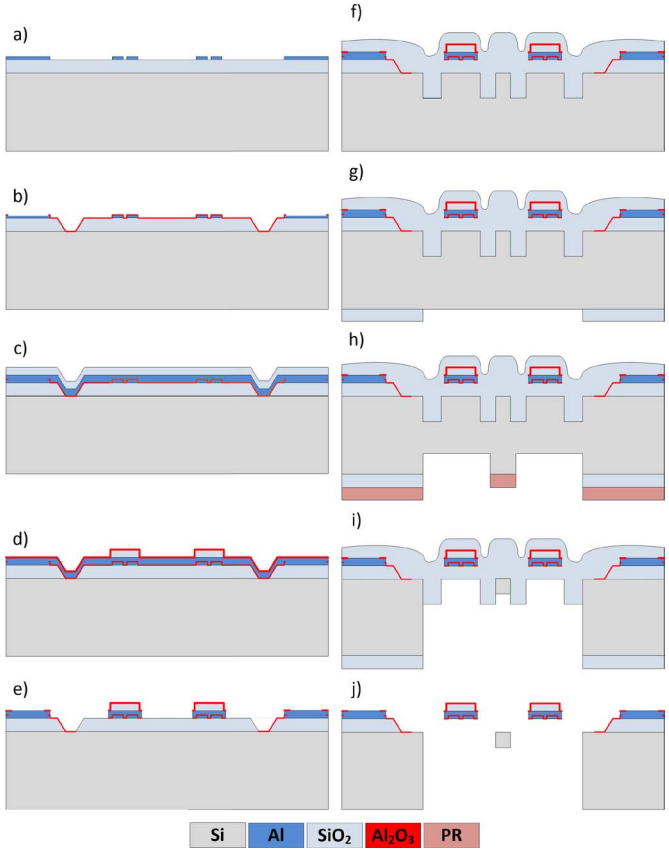

Fig. 13. Fabrication steps for bimorph definition: (a) Deposition of 3 μm-thick sacrificial SiO_2 layer, sputtering and patterning of 300 nm-thick Al film heater; (b) Wet and dry etching of the sacrificial layer, ALD for 100 nm-thick Al_2O_3 for electrical insulation and sacrificial layer protection; dry etching for contact opening; (c) Sputtering of 2 μm-thick Al and PECVD deposition of 2 μm-thick SiO_2 layer for bimorph actuators; (d) Patterning of the SiO_2 bimorph layer and deposition of 200 nm-thick ALD Al_2O_3 for vapor HF protection; (e) Dry etching of 200 nm-thick Al_2O_3 and the Al bimorph layer followed by another 100 nm-thick Al_2O_3 etching for sacrificial layer definition. (f) Front side DRIE of 15 μm silicon for hinge geometry definition, followed by deposition of low-stress 5 μm-thick stop layer; (g) Patterning of 5 μm-thick SiO_2 hard mask at the backside; (h) 50 μm DRIE etching with a photoresist mask; (i) Final DRIE etching step with SiO_2 hard mask; (j) Vapor HF device release.

Al layer sputtered at 350 °C and patterned using wet etching in PES–77–19–04 aluminum etch solution. These steps are summarized in Fig. 13a.

Next, the sacrificial layer needs to be patterned to define the area which serves as an insulator for the heater and the one which will be removed during the device release. During this step, a combination of dry plasma and wet etching is used to facilitate step coverage of the subsequent deposited layer, a 100 nm-thick atomic layer deposited (ALD) Al_2O_3, which protects the area used as insulation between the heater and the bimorph layer. Contacts are opened by dry etching in a F-based chemistry (Fig. 13b).

The bimorph layers are now defined. First, a 2 μm-thick Al layer is sputtered at 350 °C and then 2 μm of silane-based PECVD SiO_2 is added on the top (Fig. 13c). The next step is pattering of the SiO_2 bimorph layer using dry etching, followed by the deposition of 200 nm of ALD Al_2O_3 for protection of the actuators during vapor HF release (Fig. 13d).

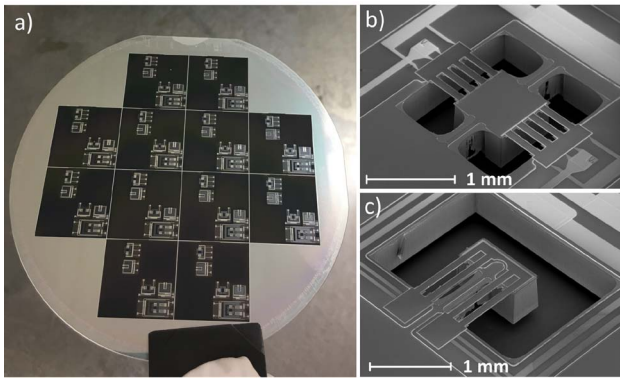

Fig. 14. (a) Optical image of a processed wafer before dicing. SEM images of (b) x direction and (c) y direction scanning MEMS actuator system before final release. Reproduced with permission form [22].

The bimorph actuators are completed by patterning by a dry etch of the Al layer and final definition of the sacrificial layer by removing unnecessary Al_2O_3 (Fig. 13e).

The hinge is defined by patterning the wafer from both sides. First, the hinge geometry is defined by front side etching of silicon (10-15 μm deep) using Deep Reactive Ion Etching (DRIE). A thick stop layer of low-stress (40 MPa) 5 μm PECVD SiO_2 is then deposited (Fig. 13f). On the backside, a 5 μm-thick PECVD SiO_2 hard mask is patterned (Fig. 13bg). Then, a two-step backside DRIE etching is done for the hinge release. The first step consists of a 50 μm deep etch (Fig. 13h), then photoresist is removed and the etch continued until approximately 10 μm of Si, the target hinge thickness, is left (Fig. 13i). Finally, the device is released by removing the sacrificial oxide and the oxide mask layers in vapor HF etch (Fig. 13j).

The fabricated devices are shown Fig. 14. A processed wafer before dicing is presented in Fig. 14a. SEM images of the MEMS actuator system for x and y direction prior to the final release of the device are given in Fig. 14b and Fig. 14c.

IV. Device Characterization

A. Electrical Characterization

The MEMS actuator systems are first characterized with a white light interferometer. The measurement principle is illustrated in Fig. 15 where d represents the distance in x or y direction for each type of scanner, respectively. The tilting and deflecting angles were calculated, for a supplied electrical input power P, based on out-of-plane displacement measurements of the microplate. The angular displacement is calculated by knowing the horizontal distance between measured points.

Measurement results for both x and y direction actuator systems are presented in Fig. 16. For the x direction scanner, a tilting range of 8° is achieved, with an average power consumption of 150 mW. No change in performance was observed even after 1000 cycles with power sweep from 0 to 300 mW in 0.1 s. For the y direction scanner, the same range is achieved with an average power consumption of 200 mW. In this case, the system was cycled for more than 5000 times with the same input signal and no changes were observed over time.

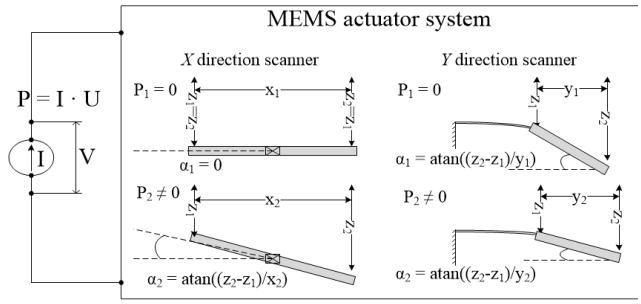

Fig. 15. Angular displacement measurement principle for (a) x and (b) y direction scanning MEMS actuator systems. Reproduced with permission form [22].

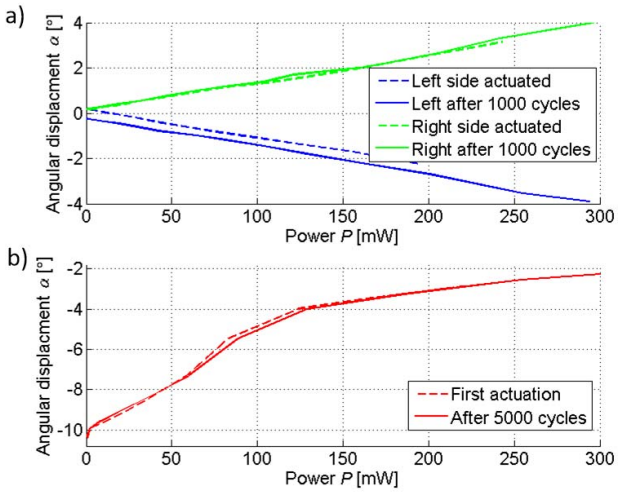

Fig. 16. Angular displacement measurement principle for (a) x and (b) y direction scanning MEMS actuator systems. Reproduced with permission form [22].

Based on simulations, the plate rotation of the actuator system for y scanning should be at the junction of the hinge and the plate. The initial angular displacement differs from the expected value. This is mainly due to the hinge thickness non-uniformity caused by a non-optimized DRIE process. Optimization of the DRIE process for this specific layout should be done to obtain better performance of the overall actuator system.

B. Thermal Characterization

The numerical simulations indicated that the MEMS actuators systems for x and for y direction scanning should reach 260 °C and 420 °C respectively, to achieve the maximum scanning range. To evaluate the bimorph temperature during static operation, first the thermal coefficient of resistance (TCR) for the bimorph heaters is characterized for each actuator system in the 25 °C to 200 °C temperature range. For each resistance measurement at a given temperature, the sample was kept for 30 minutes on the hotplate of a probe station. Then current was swept from 0 to 0.1 mA to minimize self-heating of the resistor. The characteristic presented in Fig. 17 shows a linear behavior and the temperature coefficient of resistivity was estimated to be $4.45 \pm 0.05 \times 10^{-3}$ 1/K.

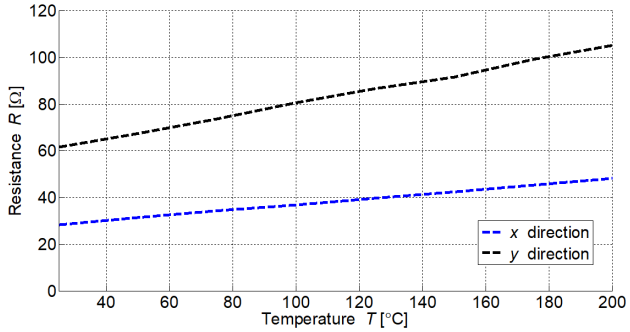

Fig. 17. Resistance versus temperature for both x and y actuator system heaters.

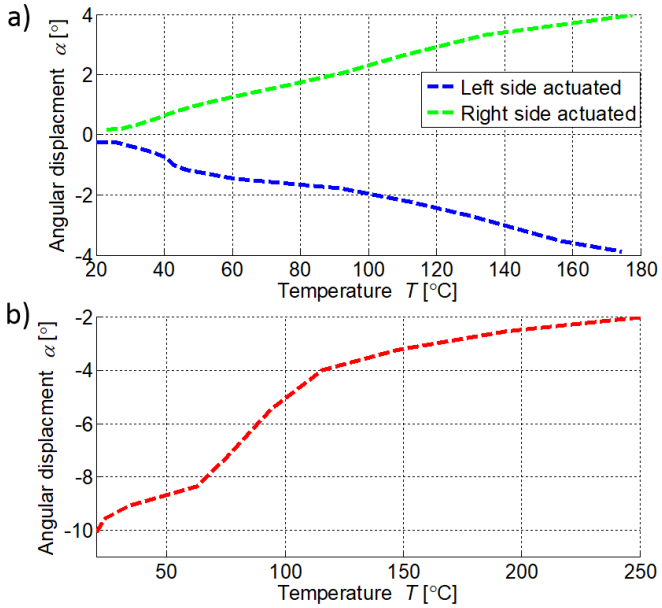

Fig. 18. Measured angular displacement versus calculated working temperature for (a) x and (b) y direction scanning MEMS actuator systems.

Knowing the initial resistance of the actuators heater, the resistance value during the actuator static operation and the thermal coefficient of resistivity, it is possible to correlate the power consumption of the MEMS actuator system with the operating temperature. The angular displacement versus calculated operating temperature for both systems is given in Fig. 18. This plot shows that the actuators did not reach the expected operating temperature. For x direction scanner, the achieved temperature is 80 °C while for y direction system it is 170 °C i.e. respectively 30% and 40% lower than calculated.

This implies there are higher temperature losses than predicted in the simulations. Supplying more than 300 mW of electrical power damaged the actuator heater. The impossibility to achieve higher temperature during the first actuation, i.e. giving higher power, results in lower initial residual stress in the beams, thus giving lower initial deflection. As a result, the actuators force F_0 is lower than expected, resulting in a lower angular displacement than predicted.

C. Frequency Response

Dynamic characteristics for both actuator systems are measured in the range 50 Hz −4 kHz using a Polytec Laser

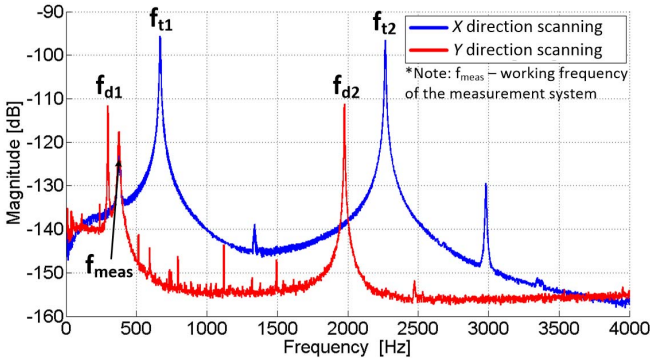

Fig. 19. Frequency response for fabricated novel MEMS actuator systems. Reproduced with permission form [22].

Doppler Vibrometer (LDV). Frequencies lower than 50 Hz were not measured to exclude electrical noise from the power supply. Results are presented in Fig. 19. The first resonant mode for the actuator systems is at 668 Hz and 297 Hz, with corresponding Q factors of 126.1 and 151.5, respectively. The higher eigenfrequency for the x direction system indicates a higher torsional stiffness. This can also explain the lower angular displacement the device has compared to the simulated value. On the other side, the deflected hinge based system has a lower frequency than calculated. The reason can be that the hinge is thinner in the middle, thus having a lower effective coefficient of elasticity. Nevertheless, the desired scanning speed for both devices is 10 Hz and therefore both scanners satisfy the dynamic requirement of 10-fold higher first mode resonant frequency.

V. Conclusion

A MEMS actuator system for an integrated self-aligned OCT scanner with Al-SiO_2 bimorph is presented. The systems are designed to translate a linear displacement of 1 cm to a rotation angle of 12°. An angular motion range of 8°, with an average power consumption of 150 mW is demonstrated. The resonant frequencies are 668 Hz and 297 Hz for x and y direction, respectively. These values are significantly higher than the 10 Hz determined by the working speed of time domain OCT. The angular motion range can be further extended by replacing the Al heater material with TiN or Mo to be able to reach the simulated temperature without heater failure. Fine tuning the DRIE process to obtain well defined hinges will be beneficial, especially for the y-direction motion.

These actuator systems are designed and fabricated to be integrated with an optical circuitry and a collimating lens in a single chip device. The integration of all components in a single chip solves one of the biggest problems for OCT systems as it provides intrinsic alignment, thus excluding coupling losses between discrete components, and simplifies packaging. Removing the need for time consuming and expensive alignment and packaging procedure is crucial in achieving a widespread use and affordability of OCT devices. The combination of the x and y direction scanning is an important step towards a single-chip 3D OCT imaging system.

ACKNOWLEDGMENTS

The authors would like to thank B. Morana, M. R. Venkatesh, L. Pakula, P. Van Holst from TU Delft and to R. Sanders from University of Twente for providing equipment and assistance with device characterization. The devices are fabricated in TU Delft-Else Kooi Laboratory (previously DIMES). The help of laboratory staff, especially S. Milosavljevic, H. van Zeijl and J.M.W. Laros is greatly acknowledged.

REFERENCES

[1] F. Erdmann *et al.*, "International trends in the incidence of malignant melanoma 1953–2008—Are recent generations at higher or lower risk?" *Int. J. Cancer*, vol. 132, no. 2, pp. 385–400, 2013.
[2] J. A. Usher-Smith, J. Emery, A. P. Kassianos, and F. M. Walter, "Risk prediction models for melanoma: A systematic review," *Cancer Epidemiol., Biomarkers, Prevent.*, vol. 23, no. 8, pp. 1450–1463, 2014.
[3] W. Drexler, "Ultrahigh-resolution optical coherence tomography," *J. Biomed. Opt.*, vol. 9, no. 1, pp. 47–74, 2004.
[4] J. Sun and H. Xie, "MEMS-based endoscopic optical coherence tomography," *Int. J. Opt.*, vol. 2011, 2011, Art. no. 825629.
[5] K. Jia, S. Pal, and H. Xie, "An electrothermal tip–tilt–piston micromirror based on folded dual S-shaped bimorphs," *J. Microelectromech. Syst.*, vol. 18, no. 5, pp. 1004–1015, Oct. 2009.
[6] S. H. Lee and Y. C. Lee, "Optoelectronic packaging for optical interconnects," *Opt. Photon. News*, vol. 17, no. 12, pp. 40–45, 2006.
[7] Y. Xu *et al.*, "Design and development of a 3D scanning MEMS OCT probe using a novel SiOB package assembly," *J. Micromech. Microeng.*, vol. 18, no. 12, pp. 12005-1–12005-8, 2008.
[8] P. Guerra, J. J. Valverde, A. Martin, M. J. Ledesma, J. L. Rubio-Guivernau, and A. Santos, "Real time signal processing and data handling with dedicated hardware in handheld OCT device," *J. Instrum.*, vol. 10, p. C11001, Nov. 2015.
[9] K. H. Kim *et al.*, "Two-axis magnetically-driven MEMS scanning catheter for endoscopic high-speed optical coherence," *Opt. Exp.*, vol. 15, no. 26, pp. 18130–18140, 2007.
[10] S. L. Medlumics, "Optical beam scanner," U.S. Patent 9 690 093 B2, Oct. 15, 2014.
[11] V. Milanovic, G. A. Matus, and D. T. McCormick, "Gimbal-less monolithic silicon actuators for tip–tilt–piston micromirror applications," *IEEE J. Sel. Topics Quantum Electron.*, vol. 10, no. 3, pp. 462–471, May/Jun. 2004.
[12] D. J. Bell, T. J. Lu, N. A. Fleck, and S. M. Spearing, "MEMS actuators and sensors: Observations on their performance and selection for purpose," *J. Micromech. Microeng.*, vol. 15, no. 7, pp. S153–S164, 2005.
[13] H. J. Cho and C. H. Ahn, "Magnetically-driven bi-directional optical," *J. Micromech. Microeng.*, vol. 13, no. 3, pp. 383–389, 2003.
[14] W.-K. Jeung, S.-M. Choi, and Y.-J. Kim, "Large displacement polymer bimorph actuator for out-of-plane motion," *J. Elect. Eng. Technol.*, vol. 1, no. 2, pp. 263–267, 2006.
[15] Y. Zhang, Y. Zhang, and R. B. Marcus, "Thermally actuated microprobes for a new wafer probe card," *J. Microelectromech. Syst.*, vol. 8, no. 1, pp. 43–49, 1999.
[16] L. Wu and H. Xie, "124° rotation angle electrothermal micromirror with integrated platinum heater," *J. Sel. Topics Quantum Electron.*, vol. 13, no. 2, pp. 316–321, 2007.
[17] C. Duan, W. Wang, X. Zhang, L. Zhou, A. Pozzi, and H. Xie, "A 45°-tilted two-axis scanning micromirror for side-view imaging," *J. Microelectromech. Syst.*, vol. 25, no. 4, pp. 799–811, Aug. 2016.
[18] S. R. Samuelson and H. Xie, "Electrothermally actuated large displacement waveguides," in *Proc. Int. Conf. Opt. MEMS Nanophoton. (OMN)*, Kanazawa, Japan, 2017, pp. 109–110.
[19] K. Solehmainen *et al.*, "Dry-etched silicon-on-insulator waveguides with low propagation and fiber-coupling losses," *J. Lightw. Technol.*, vol. 23, no. 11, pp. 3875–3880, Nov. 2005.
[20] D. Resnik, D. Vrtacnik, U. Aljancic, M. Mozek, and S. Amon, "The role of Triton surfactant in anisotropic etching of {1 1 0} reflective planes on (1 0 0) silicon," *J. Micromech. Microeng.*, vol. 15, no. 6, pp. 1174–1183, 2005.
[21] A. Jovic, G. Pandraud, K. Zinoviev, J. L. Rubio, E. Margallo, and P. M. Sarro, "Fabrication process of Si microlenses for OCT systems," *Proc. SPIE*, vol. 9888, p. 98880C, 2016.
[22] A. Jovic *et al.*, "Two novel MEMS actuator systems for self-aligned integrated 3D optical coherent tomography scanners," in *Proc. IEEE 30th Int. Conf. Micro Electro Mech. Syst. (MEMS)*, Las Vegas, NV, USA, Jan. 2017, pp. 797–800.
[23] C. Liang and B. C. Prorok, "Measuring the thin film elastic modulus with a magnetostrictive sensor," *J. Micromech. Microeng.*, vol. 17, no. 4, pp. 709–716, 2007.
[24] B. Rashidian and M. G. Allen, "Electrothermal microactuators based on dielectric loss heating," in *Proc. IEEE Micro Electro Mech. Syst.*, 1993, pp. 24–29.
[25] R. B. McLellan and T. Ishikawa, "The elastic properties of aluminum at high temperatures," *J. Phys. Chem. Solids*, vol. 48, no. 7, pp. 603–606, 1987.

Aleksandar Jovic was born in Bor, Serbia, in 1989. He received the B.Sc. and M.Sc. degrees in electrical engineering from the University of Belgrade, Serbia, in 2012 and 2013, respectively. He is currently pursuing Ph.D. degree with the ECTM Group, Delft University of Technology, and is involved in design, fabrication, and characterization of MEMS devices. In 2018, he joined the Else Kooi Laboratory as a Senior Patterning Engineer responsible for dry etching and lithography processes.

Grégory Pandraud received the Ph.D. degree in optics and optoelectronics from the University of Saint Etienne, France, in 1998. He joined the University of Twente, The Netherlands, as a Post-Doctoral Fellow for one year. From 1999 to 2002, he was a Development Engineer at Bookham Technolgies plc., U.K., and a Senior Design Manager at Opsitech S.A., France, where he developed integrated optical components for DWDM and next generation networks applications. In 2003, he joined as a Senior Researcher with the Else Kooi Laboratory, where he is currently a Manager of the Else Kooi Laboratory.

Nuria Sanchez Losilla received the Ph.D. degree in physics with over ten years' experience in research and development. The last five years in nanophotonics area as a Research and Development Engineer in a cleanroom environment, she has been responsible for technology development and manufacturing activities at wafer level of photonic devices based on silicon photonics. The first five years of her scientific research in the field of bionanotechnology, she has conducted experimental work in the development of biosensors and new microscopies. She was involved in numerous research and development national and European projects formed by multidisciplinary teams. She is an author of 17 publications in international journals and over 20 contributions in congresses.

Juan Sancho received the M.Eng. and Ph.D. degrees in technologies, systems, and communication, and the M.Sc. degree in telecommunication engineering from the Polytechnic University of Valencia (UPV), Spain. He has ten years of experience in the field of optics, telecommunications, instrumentation, signal processing, photonic circuit design, simulation, characterization, and manufacturing. He has been involved in several European and national projects to expand the current capabilities in the photonic field for real-world applications. In the past five years, he was focused on biomedical field developing Medlumics's photonics platform. He has managed the key projects in company and is leading the photonics area.

Kirill Zinoviev received the M.Sc. degree in electrical engineering from Vladimir State University, Murom, Russia, in 1994, and the Ph.D. degree in engineering from the State Academy of Engineering, Moscow, Russia, in 1997. He is currently with imec, Belgium. His research interests include the design, fabrication, and characterization of the sensors based on integrated optics and fabricated using silicon technologies.

Jose Luis Rubio received the M.Eng. degree in telecommunications and the Ph.D. degree in biomedical imaging from the Polytechnic University of Madrid. In the past eight years, he was involved in the modeling and simulation of biomedical imaging systems, advanced reconstruction algorithms, and in the processing of medical images. He has participated in several projects in these areas, both at national and European levels, and was with universities, research centers, and hospitals in Spain, France, and U.S. He received the MIT Technology Review Award for main innovators under 35 in Spain. He co-founded MedLumics in 2009, where he is currently a Chief Technology Officer.

Eduaro Margallo-Ballbas received the M.Eng. degree in telecommunications from the Polytechnic University of Madrid, the M.Sc. degree in physics from UNED, the M.Eng. degree in electrical engineering (Dipl.-Ing. Elektrotechnik) from the University of Stuttgart, Germany, and the Ph.D. degree in biophotonic instrumentation from the Delft University of Technology, The Netherlands. He has eight years of experience in the design and manufacturing of biophotonic instrumentation and integrated optics, with in-depth knowledge of the physics of light propagation in tissue, sensor microfabrication techniques, and silicon photonic devices. During this time, he has participated in the definition and implementation of clinically driven research projects in collaboration with several universities and hospitals in The Netherlands and Italy. He co-founded MedLumics in 2009, where he is currently a Chief Operating Officer, having guided the company through its seed and start-up phases. In particular, he led fund-raising activities resulting in a 34,4M€ in private investments.

Pasqualina M. Sarro (M'83–SM'97–F'07) received the Laurea degree (*cum laude*) in solid-states physics from the University of Naples, Italy, in 1980, and the Ph.D. degree in electrical engineering from the Delft University of Technology, The Netherlands, in 1987. From 1981 to 1983, she was a Post-Doctoral Fellow in the Division of Engineering, Photovoltaic Research Group, Brown University, Providence, RI, USA. She joined the EE Faculty, Delft University of Technology, to establish and lead research on silicon micromachining, integrated sensor, MEMS, and material processing. In 2001, she was an appointed Antoni van Leeuwenhoek Full Professor for research merits. She has (co)-authored over 500 publications. Her main research interests include novel materials and structures for MEMS and NEMS to be applied in health, automotive, environmental applications, and scientific instrumentation. She is a member of the International Steering Committee of Eurosensors, Transducers, and IEEE MEMS. She serves on various international advisory boards and panels for research. She is an elected member of the Royal Netherlands Academy of Sciences, a Knight in the Order of the Dutch Lion, and a Knight in the Order of the Italian Star. She was the General Chair and the Technical Program Committee Chair for all major international conferences in the field of sensors, MEMS, and microsystems several times. From 2006 to 2009, she was an Associate Editor for the IEEE SENSORS JOURNAL. She is an Associate Editor for the IEEE JOURNAL OF MICROELECTROMECHANICAL SYSTEMS.